A Multimodal, Enveloping Soft Gripper: Shape Conformation, Bioinspired Adhesion, and Expansion-Driven Suction

Yufei Hao, Shantonu Biswas, Elliot Wright Hawkes, *Member, IEEE*, Tianmiao Wang, Mengjia Zhu, Li Wen, and Yon Visell, *Member, IEEE*

***Abstract*—A key challenge in robotics is to create efficient methods for grasping objects with diverse shapes, sizes, poses, and properties. Grasping with hand-like end effectors often requires careful selection of hand orientation and finger placement. Here, we present a fingerless soft gripper capable of efficiently generating multiple grasping modes. It is based on a soft, cylindrical accordion structure containing coupled, parallel fluidic channels, which are controlled via pressure supplied from a single fluidic port. Inflation opens the gripper orifice for enveloping an object, while deflation allows it to produce grasping forces. The interior is patterned with a gecko-like skin that increases friction, enabling the gripper to lift objects weighing up to 20 N. Our design ensures that fragile objects, such as eggs, can be safely handled, by virtue of a wall buckling mechanism. In reverse, the gripper can be deflated to reach into an opening or orifice then inflated to grasp objects with handles or cavities. The gripper may also integrate a lip that enables it to form a seal and, upon inflating, to generate suction for lifting objects with flat surfaces. In this article, we describe the design and fabrication of this device and present an analytical model of its behavior when operated from a single fluidic port. In experiments, we demonstrate its ability to grasp diverse objects, and show that its performance is well described by our model. Our findings show how a fingerless soft gripper can efficiently perform a variety of grasping operations. Such devices could improve the ability of robotic systems to meet applications in areas of great economic and societal importance.**

***Index Terms*—Bioinspired adhesion, shape conformation, soft gripper, suction.**

Manuscript received April 23, 2020; revised July 1, 2020; accepted August 24, 2020. The work of Y. Hao was supported by the China Scholarship Council fund under Grant 201806020091. The work of Y. Visell was supported by the U.S. National Science Foundation under Grant NSF-1628831, Grant NSF-1623459, and Grant NSF-1751348. This paper was recommended for publication by Associate Editor H. Wang and Editor P. Dupont upon evaluation of the reviewers' comments. *(Corresponding authors: Yufei Hao; Yon Visell.)*

Yufei Hao is with the School of Mechanical Engineering and Automation, Beihang University, Beijing 100083, China, and also with the Soft Transducers Laboratory, Ecole Polytechnique Fédérale de Lausanne, 1015 Lausanne, Switzerland (e-mail: by1407140@buaa.edu.cn).

Tianmiao Wang and Li Wen are with the School of Mechanical Engineering and Automation, Beihang University, Beijing 100083, China (e-mail: itmlab@sina.com; liwen@buaa.edu.cn).

Shantonu Biswas is with the California NanoSystems Institute, University of California, Santa Barbara, Santa Barbara, CA 93106 USA (e-mail: sbiswas@ucsb.edu).

Elliot Wright Hawkes is with the Department of Mechanical Engineering, University of California, Santa Barbara, Santa Barbara, CA 93106 USA (e-mail: ewhawkes@engineering.ucsb.edu).

Mengjia Zhu and Yon Visell Wen are with the Media Arts and Technology Program, Department of Electrical and Computer Engineering, University of California, Santa Barbara, Santa Barbara, CA 93106 USA (e-mail: mengjiazhu@ucsb.edu; yonvisell@gmail.com).

This article has supplementary downloadable material available at https://ieeexplore.ieee.org, provided by the authors.

Color versions of one or more of the figures in this article are available online at https://ieeexplore.ieee.org.

Digital Object Identifier 10.1109/TRO.2020.3021427

I. Introduction

ROBOTIC grasping is challenging in many applications, especially those that involve objects with varying sizes, shapes, poses, and properties. This has motivated the development of a variety of hand-like robotic grippers with multiple fingers [1]. It has also led to the development of proprioceptive, force, and torque sensors and algorithms and hardwares for robotic perception of objects' shape, pose, and properties, for planning and controlling robotic grasping, and achieving form/force closure [2], [3]. Such grasping processes often involve computational scene perception and understanding, or online sensor feedback [4]. The uncertainties arising in practical applications, and the limited compliance of many grippers, make it especially challenging for robotic systems to handle fragile, unfamiliar, or brittle objects.

Recent research on soft robotic grippers has led to several new proposals for improving robotic grasping [5]. Compared to rigid grippers, soft grippers ensure compliant interactions with objects due to their intrinsic compliance. They may be fabricated using techniques that are amenable to multimaterial customization, including casting methods based on two component liquid polymers. This has also led to many approaches to actuation, which include electroactive polymer [6]–[8], electromagnetic [9], [10], thermal or light reaction [11]–[13], chemical stimulation [14], [15], and fluidic actuation via differential pressure [16]–[18].

Pneumatic grippers, which are often made of cast silicone elastomers, have been widely investigated because of their low cost, easy manufacturing, high performance, and environmental robustness. They have been deployed in both terrestrial operation [19] and underwater sampling [20], [21]. More degrees of freedom can be introduced in such grippers through the use of multiple, separated air chambers, or by preprogramming bending locations via functional materials, which can improve the adaptability of a gripper to objects of different sizes and shapes [22]–[24]. The load capacity of such grippers can be improved by employing variable stiffness structures and mechanisms, including materials of greater or adjustable rigidity [25]–[29].

These improvements can significantly enhance grasping performance.

However, both soft and rigid fingered grippers present challenges in robotic grasping, due to the discrete contacts produced by the fingers and bending mode of actuation. For example, a fingered gripper may generate a reverse moment at the contact point when touching objects, which may push the fingers away from the objects. And gaps between the fingers and the target object cannot be eliminated, which may inhibit grasping stability. Further equipping such grippers with auxiliary actuation systems, such as suction cups, can enhance grasp stability at the expense of greater complexity[30]–[33]. In most cases, when grasping an object, a robot using fingered grippers must account for the positions and orientations of the fingers in relation to the geometry and pose of an object in order to determine a feasible grasping solution.

Vacuum-driven, nonfingered grippers based on granular jamming or the origami design, can overcome some of these limitations by conforming to objects of arbitrary shapes [34]–[36]. However, such devices can only grasp objects by vacuuming to contract the membrane to conform the gripper around the object, limiting them to a single grasping mode. In addition, achieving higher holding forces with such grippers requires greater (negative) pressures, which may pose problems when they manipulate very fragile objects.

Suction is another useful gripping strategy that does not involve enveloping. Many suction grippers have been developed. Inspiration from the suckers of octopus, clingfish, and remora have motivated designs that achieve improved suction forces and adhesion to cambered or rough surfaces [37]–[39]. Related engineering technologies, such as electroadhesion and shape reconfiguration, have also been used to improve the performance of such grippers [40], [41]. However, the application of suction-based grippers is often limited to objects with flat or nearly flat surfaces.

In this article, we present a simple but multifunctional fingerless soft gripper that is able to grasp objects in a variety of poses, sizes, and shapes. The gripper consists of an array of parallel chambers in a soft accordion structure that forms a cylindrical aperture. It is controlled via pressure supplied from a single fluidic port. With this single control input, the gripper is able to produce three different compliant grasping behaviors. In the first mode (contraction-based grasping), inflation opens the orifice of the gripper for enveloping an object to be grasped. Subsequently, deflating it envelops the object and produces grasping forces. The lifting capacity is improved via a bioinspired, gecko-like patterned skin, increasing the shear force. The design facilitates a wall buckling mechanism that ensures that fragile objects, such as eggs, can be safely handled. In the second grasping mode (expansion-based grasping), the gripper can inflate to expand into an opening or orifice for grasping objects with handles or openings. The third grasping mode (expansion-driven suction) is enabled by augmenting the gripper with a lip that enables it to form a seal with flat objects. Subsequently inflating the gripper (and thereby expanding the interior region) produces a suction that enables the gripper to lift objects via flat surfaces.

The structure of this article is as follows. We first describe the structure and implementation of this device, then present a design analysis describing the gripper expanding radius with the relationship of applied pressure and the number of chambers. In a series of experimental results, we verify the analysis with experiments, explain how the gripper ensures grasping performance and safety, demonstrate its ability to grasp diverse objects by adapting to their shapes, and characterize the forces produced by the gripper and other performance attributes in each of the three grasping modes. We then analyze the predictive ability of the analytical model, the characteristics of the gripper, and the failure cases for grasping, before concluding. The contributions of this work include a new method and device for grasping a variety of objects by passively adapting to their shapes, methods for producing several different grasping behaviors via the same soft gripper, and a method of grasping that can simultaneously achieve high load capacity via gecko-like adhesion and safely handling of fragile objects by virtue of a wall buckling property.

II. Structure and Implementation

The structure of the gripper is based on a cast silicone main body that enables the gripper to perform multifunctional grasping via a single fluidic port (see Fig. 1). The gripper is composed of a main accordion structure, which contains 22 parallel chambers connected to a single fluidic port, and three fasteners, which are used to seal, inflate, and deflate the gripper [see Fig. 1(a2)]. To increase the load capacity of the gripper, we add a gecko-like skin to the inner surface [see Fig. 1(a3)]. The gecko-like skin has multiple lines of micro wedges. In its default, unloaded state, only the tips of the wedges touch an object. However, when loaded in shear, the wedges lay over, and the real area of contact greatly increases, producing adhesion[42]. This adhesion creates an adhesion-controlled friction force, similar to the familiar load-controlled friction force, but created by the adhesion force instead of the normal force. It is this adhesion-controlled friction force that we levarge to increase the shear force capabilities of our gripper. Functionally, the use of microwedges means very little normal force needs to be applied to achieve a significant shear force. The chambers form a cylindrical aperture. Each has a width of 6 mm, a length of 9.2 mm [see Fig. 1(b2)], a height of 65 mm [see Fig. 1(a2)], and a wall thickness of 1.2 mm. To facilitate the contraction and expansion motions of the gripper, we designed the chambers with a honeycomb-like shape that guarantees their anisotropic motion. Under deflation, the chambers can easily fold along the circumferential direction, causing the aperture to shrink to a smaller circumference [see Fig. 1(a1) and (b1)]. Under inflation, the chambers expand primarily in the circumferential direction, rather than in the radius direction. This causes the aperture to expand, producing a shape similar to that of a lotus flower [see Fig. 1(a3) and (b3)]. The motion of the gripper is also illustrated in Supplementary Video S1. These inflation and deflation behaviors enable two modes of grasping, based on contracting around an object or inflating within an object aperture. Application of positive pressure enables the gripper to “swallow” the object, while subsequent application of negative pressure causes it to envelop and conform to the object

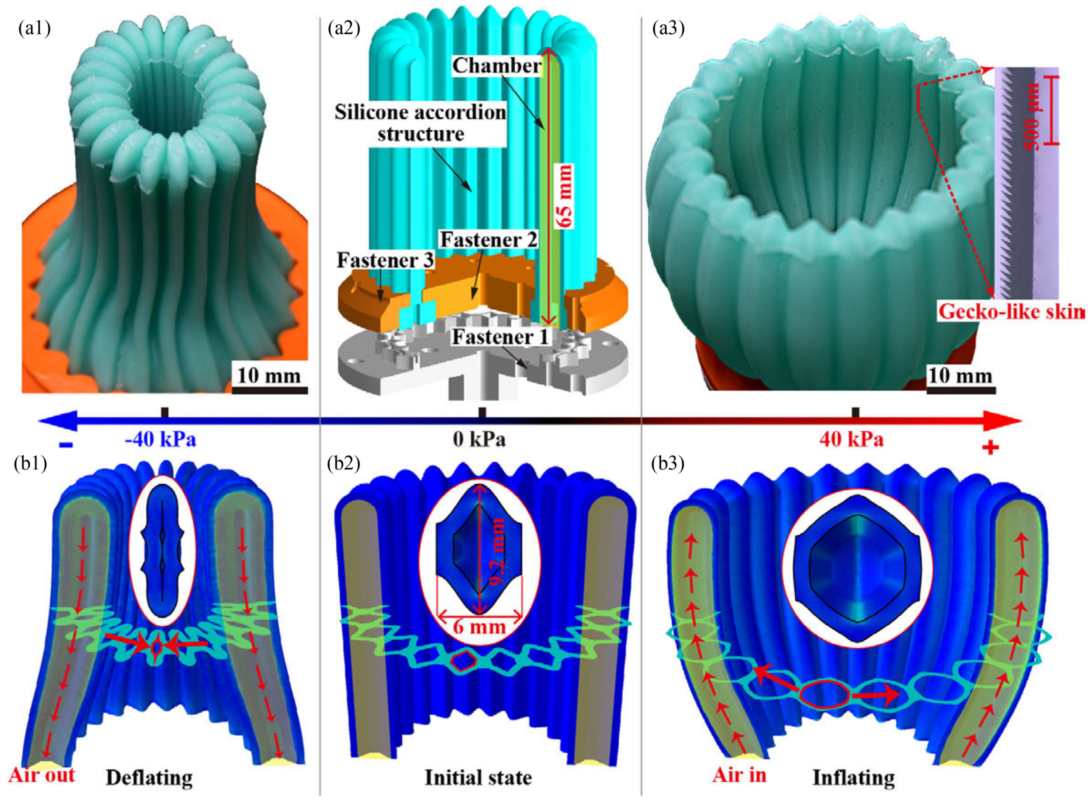

Fig. 1. Design and operating principle of the gripper. (a1) Gripper contracts as pressure is decreased, closing the aperture. (a2) This is enabled via an array of 22 parallel channels embedded in a silicone accordion structure, all connected to a common fluid port. (a3) Inflating the gripper causes it to expand, exposing the gecko-like skin covering the interior region. (b1) Negative differential pressures, contraction is produced via folding of the soft accordion structure. The inset panel shows the folding motion of one chamber. (b2) State of the gripper without any input pressure change. The inset panel shows the dimension of the rested chamber. (b3) Expansion of the gripper is produced through positive pressure supplied to the channels, which causes the accordion structure to spread. The inset panel shows the expanding motion of one chamber.

for lifting. This process is reversed in the interior grasping mode, for which the gripper is first deflated to insert into an aperture in the object, then expanded in order to grasp it.

The gripper is primarily molded from low viscosity platinum catalyzed silicone polymer (Mold Star 15, Smooth-On Inc., USA). The fabrication process is illustrated in Fig. 2. We first prepare all the ABS molds for the gripper using 3D printing (Stratasys F270, Objective3D, Australia). Then, we transfer print the gecko-like skin, which is prefabricated via a micro-machined mold with a patterned texture [43], onto the wall of the shaft mold [see Fig. 2(a)] via dry adhesion. Subsequently, we assemble the shaft mold, chamber mold, and shell mold together and fill it with uncured silicone rubber, which is made by mixing the polymer resin binary components in equal volume. After degassing in a vacuum container for thirty minutes, we place a cover on top of the mold assembly and allow it to cure for eight hours. A small amount of excess silicone rubber is expelled through the riser [see Fig. 2(b)].

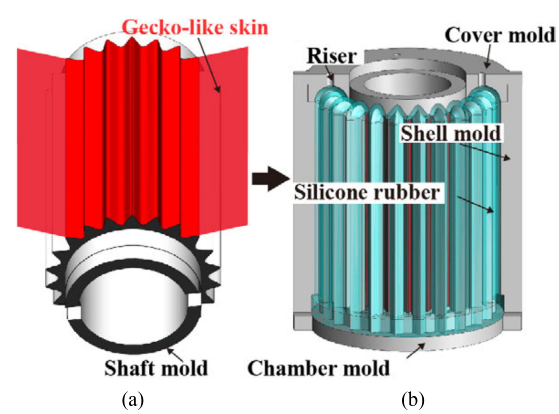

Fig. 2. Fabrication of the gripper is based on a multipart casting procedure. (a) Transfer printing is used to apply the patterned gecko-like skin to the surface of the shaft mold. (b) After assembling the chamber mold, shell mold, and shaft mold, uncured liquid silicone rubber is poured into the mold assembly, which is completed via a cover mold.

III. Design Analysis

The workspace of the gripper determines the smallest and largest objects it can grasp. The smallest object that can be grasped is determined by the minimum gripper aperture, which depends on the number and dimensions (principally thickness) of the chamber. The largest graspable object size is determined by the maximum gripper aperture, which occurs at a pressure for which the accordion structure becomes maximally unfolded.

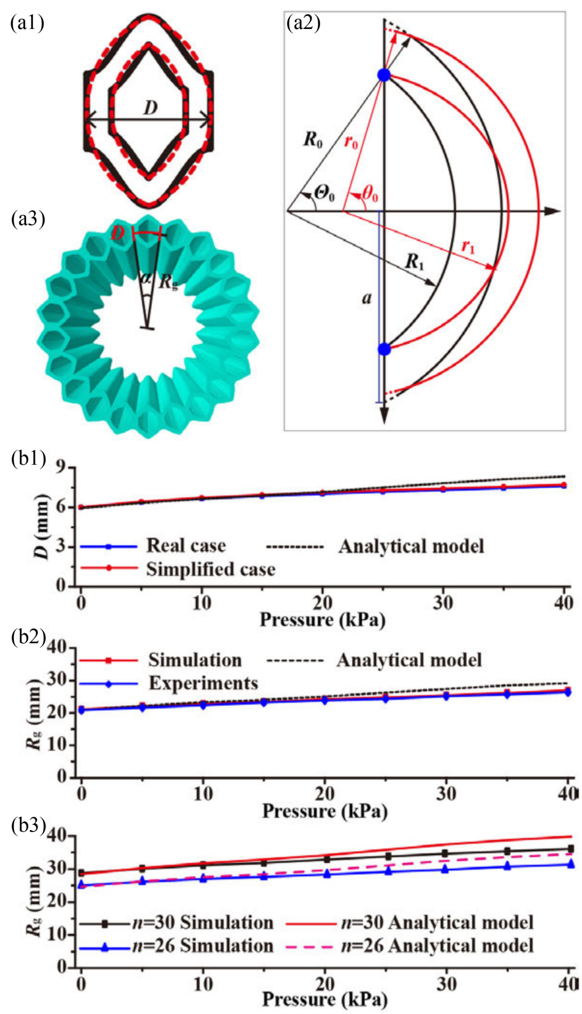

Fig. 3. Predictions of the analytical model, numerical simulation, and measured behavior of the gripper as functions of fluid pressure. (a1) Matching single chamber geometry to the model, section views. Black profile: True geometry. Red dashed profile: Approximation via circular arcs tangent to the chamber. D: Interior distance. (a2) Simplified geometry of the half wall of one chamber as used in the analytical model. (a3) Geometric relationship of the deformed gripper. R_g is the gripper aperture radius. (b1) Comparison of D for simulation models (Real case and Simplified case) and the analytical model for pressures from 0 to 40 kPa. (b2) Comparison of gripping aperture size versus pressure for the simulation, analytical model, and measurements for a gripper prototype $n = 22$. (b3) Comparison of grip aperture size versus pressure for the simulation and analytical model when $n = 26$ and 30.

We develop an analytical model to analyze the diameter of the gripper as a function of applied pressure. Because all chambers have the same geometry, we first establish a relationship between the pressure and the distance between the side walls of a single chamber [see D in Fig. 3(a1)], and extrapolate from this to determine the shape of the entire gripper aperture.

The geometry of the chamber [black profile in Fig. 3(a1] is complex, so we approximate the profile via circular arcs that capture the characteristic deformation [red dashed profile in Fig. 3(a1)]. For this simplified case, the arcs are tangent to the wall of the chamber at the midpoint. For reasons of symmetry, we can focus on half of the chamber [see Fig. 3(a2)]. For moderate pressures, the walls undergo little stretching, so we ignore the strain along the height of the walls, and assume that the cross section area of the chamber section remains constant. Considering the top and bottom points of the inner surface [blue points in Fig. 3(a2)] displace little vertically when the pressure is under 40 kPa, we constrain these points to be fixed in space for modeling simplicity. We refer to the uninflated inner and outer radii as R_1 and R_0, respectively, and the half central angle as Θ_0. After inflation, the inner radius, outer radius, and half central angle change to r_1, r_0, and θ_0, respectively. The principle strain in the θ direction is

$$\lambda_\theta = r\theta_0/(R\Theta_0). \tag{1}$$

Because we assume that the material is incompressible, the principle strain in the r direction is

$$\lambda_r = R\Theta_0/(r\theta_0). \tag{2}$$

Applying the Cauchy equilibrium equations, we obtain

$$d\sigma_{rr}/dr = (\sigma_{\theta\theta} - \sigma_{rr})/r \tag{3}$$

where σ_{rr} is the stress in the r direction, and $\sigma_{\theta\theta}$ is the stress in the θ direction. Force balance in the r direction implies that

$$P = \int_{r_1}^{r_0} (\sigma_{\theta\theta} - \sigma_{rr})/r \; dr \tag{4}$$

where P is the inflating pressure.

The relationship between stress and strain is determined by the material properties. Here, we adopt an incompressible, neo-Hookean model for the elastomer (Mold Star 15) [44]. The strain energy density function for the material is

$$W = C_1(I_1 - 3) \tag{5}$$

where C_1 is a material constant with a value of 119 kPa [44], and I_1 is the first invariant of the left Cauchy-Green deformation tensor

$$I_1 = \lambda_1^2 + \lambda_2^2 + \lambda_3^2. \tag{6}$$

The Cauchy stress difference for $\sigma_{\theta\theta}$ and σ_{rr} is given by

$$\sigma_{\theta\theta} - \sigma_{rr} = \lambda_\theta(\partial W/\partial\lambda_\theta) - \lambda_r(\partial W/\partial\lambda_r) \tag{7}$$

where $\partial W/\partial\lambda_\theta = 2C_1\lambda_\theta$, and $\partial W/\partial\lambda_r = 2C_1\lambda_r$. Substituting these two equations into (7), we obtain

$$\sigma_{\theta\theta} - \sigma_{rr} = 2C_1\lambda_\theta^2 - 2C_1\lambda_r^2. \tag{8}$$

The deformation of the chamber is described by

$$(R^2 - R_1^2)\Theta_0 = (r^2 - r_1^2)\theta_0. \tag{9}$$

Substituting (1), (2), (8), and (9) into (4), we obtain

$$P = 2C_1\frac{\theta_0}{\Theta_0}\ln\frac{R_0}{R_1} + C1\frac{\Theta_0}{\theta_0^2}(R_1^2\Theta_0 - r_1^2\theta_0)\left(\frac{1}{r_0^2} - \frac{1}{r_1^2}\right) - C_1\frac{\Theta_0}{\theta_0}\ln\frac{r_0}{r_1}. \tag{10}$$

The edges [blue points in Fig. 3(a3)] are fixed, thus

$$r_1 \sin\theta_0 = a \tag{11}$$

where a is half of the initial distance between the two end points. The cross-sectional area may be assumed to be constant

$$(R_0^2 - R_1^2)\Theta_0 = (r_0^2 - r_1^2)\theta_0. \tag{12}$$

Solving the nonlinear set of (10)–(12), yields expressions for r_0, r_1, and θ_0. We solved these numerically. In order to find solutions matching our configuration, we restricted their ranges to values near our design, i.e.,

$$\begin{aligned} r_0 &\in [4.56, 5] \\ r_1 &\in [3, 3.8] \\ \theta_0 &\in [57.6°, 80°]. \end{aligned} \tag{13}$$

The expression for the wall distance *D* is then given by

$$D = 2(r_0 - r_1 \cos\theta_0). \tag{14}$$

Because the gripper is composed of identical chambers, when it is inflated, the arc length of one chamber *D* and the radius R_g increase, while the central angle α remains constant [see Fig. 3(a3)]. From this, the relationship between *D* and R_g can be deduced to be

$$R_g = D/\alpha. \tag{15}$$

Here, *D* is used to approximate the length of the arc, based on Fig. 3(a1), and $\alpha = 360°/n$, where *n* is the number of the chambers. For the tested prototype $n = 22$.

IV. Results

A. Design Analysis

To assess the validity of the analytical model, we compared the analytical results *D* for one chamber with simulation results for the true and simplified geometries described previously [see Fig. 3(b1)]. Results for the simplified geometry exhibited little deviation from those for the true geometry, confirming that the simplification approximates the real deformation. The resulting analytical model exhibits excellent agreement with the FEA simulation for pressures below 20 kPa. The maximum error is approximately 0.04 mm. Larger errors occur at higher pressures. We then compared the predicted dependence of R_g on pressure with the FEA simulation and laboratory experiments. For the FEA simulation, we inflated the gripper to different pressures and determined the coordinates of the center points of the chambers. We used these coordinates to fit the corresponding circles, and used this to calculate the values of R_g. For the experiments, we inflated the gripper to specified pressures and measured the deformed shape. After digitizing the center points of the chambers in software, we calculated values of R_g. Results from Fig. 3(b2) shows that the maximum error for the simulation in comparison with the experiments is 0.49 mm, demonstrating good agreement between the simulation and the experiments. For the analytical model, the error was less than 1.2 mm for pressures below 20 kPa. However, as in the case analyzed previously, the error increases with increasing pressure. To verify the universality of the analytical model, we changed the number of chambers, *n*, to 26 and 30, and compared the calculated values of R_g with those for simulation. Results from Fig. 3(b3) reveal that, for both $n = 26$ and 30, the analytical model performance is similar to the case $n = 22$, i.e., the errors increase when the pressure is above 20 kPa. We hypothesize that the errors may be attributable to our simplifying assumption that the specified geometric points remained stationary, since these points may have displaced at higher pressures. Interactions between the neighboring chambers may also have played a role, because the fasteners impede their free motion at those locations.

B. Passive Shape Conformation, Wall Buckling, and Gecko-Inspired Adhesion

The ability of the gripper to passively conform to objects of various sizes, shapes, and poses facilitates grasping. Grasping with fingered grippers often produces gaps, due to the geometry and bending action of the fingers [see Fig. 4(a1)]. For such grippers, the orientations of the fingers and objects must be accounted for in order to achieve stable grasping [see Fig. 4(a2)]. In contrast, our gripper can readily conform to objects in various shapes, sizes, and poses by passively adapting to their shapes [see Fig. 4(a3) and (g)]. When the gripper is actuated to grasp an object, points on the gripper surface stay in place upon contacting the object, while other surface points on the gripper continue to move until they touch the object. In the contaction-based mode, the gripper can adapt to the shape of a variety of objects; Fig. 4(b1)–(d2) demonstrate adaptation to rectangular and hexagonal pyramids or cones, even when these objects are placed upside down. The gripper can also grasp objects with concave surfaces [see Fig. 4(c)]. In the expansion-based grasping mode, the gripper can be inserted into an orifice and inflated to conform to the apertures of objects, such as cups [see Fig. 4(f)] or hollow cubes [see Fig. 4(g)]. It is challenging to achieve similar levels of shape adaptation via fingered grippers.

The softness of most soft grippers ensures safe operation but limits their load capacity. In contrast, our device can safely grasp brittle objects without excessive decrease the load by virtue of the synergistic combination of wall buckling and gecko-like adhesion properties that are integrated in the design. As [see Fig. 5(a)] shows, the normal force, measured via the force transducer (ATI F/T Sensor Nano 17) integrated with the gripper, increases when the gripper is deflated to conform the object. However, the normal force plateaus as pressure is decreased further, due to the collapse of the pneumatic chambers in the walls. This wall buckling prevents the gripper from damaging fragile objects, such as eggs [see Fig. 5(c)], even under the application of large negative pressures. Nonetheless, the gecko-like skin that patterns the interior surface ensures that the shear force of the gripper is sufficient to lift objects many times heavier than the gripper itself, up to 2 kg in mass [see Fig. 5(b)]. The safety and load capacity of the gripper are further illustrated in Supplementary Video S2.

C. Lifting Forces During Contraction-Based Grasping

We conducted experiments to assess the dependence of the lifting forces on the size and shape of objects, and the actuating pressure for the contraction-based grasping mode. Fig. 6(a1) shows that the lifting force increases quickly then decreases

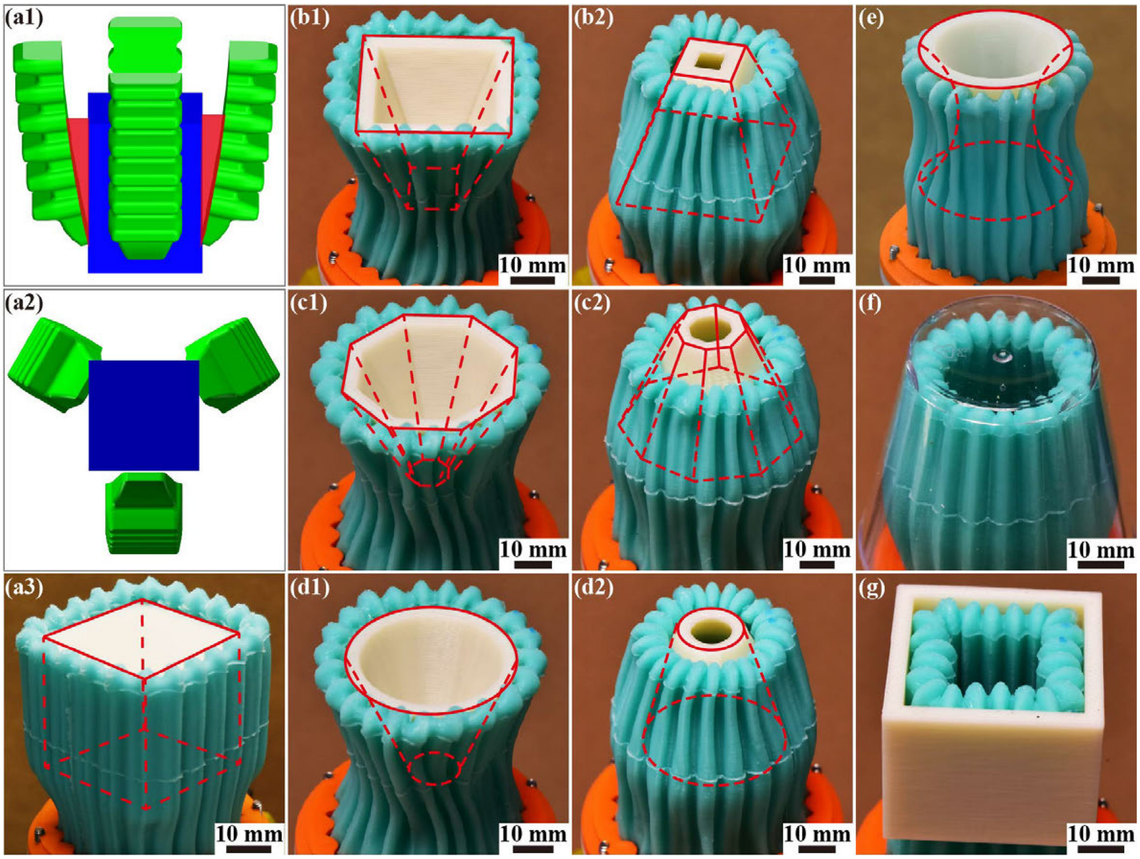

Fig. 4. Performance of our gripper is facilitated by its ability to passively conform to the shape of grasped objects. It can be compared with grasping via fingered grippers, (a1) which often involve gaps between the fingers and object, (a2) also demand that the object configuration and finger poses be accounted for, limiting the range of feasible grasp poses. (a3) In contrast, our gripper can readily conform to the shape of the object. Using our enveloping method, many object shapes can be grasped, such as (b1) a rectangular pyramid, (c1) a hexagonal pyramid, or (d1) a cone. The same objects can be grasped when inverted (b2), (c2), and (d2). The gripper can also conform to objects with concave shapes (e). By expanding into an orifice, the gripper can grasp objects via their interior, such as (f) a cylinder or (g) cube.

slowly as a cylinder detaches from the gripper. For all sizes of cylinder, the pressures required for lifting are identical (-30 kPa). During lifting, micro wedges on the gecko-like skin incline to ensure that the load is evenly shared across a large contact area, enabling larger shear forces to be produced by friction [42]. The maximum forces produced increased with the diameter of the object, from 32 to 48 mm, because the contact surface area increases with increasing diameter. Fig. 6(a2) shows that a modest increase in maximum attained lifting forces accompanies a deflation of the gripper from 0 to -20 kPa, with little further change under augmentation of vacuum. This is due to the buckling of the wall chambers. (It should be noted that the data for the 32 mm diameter under 0 kPa is missing because the gripper failed to contact the object.)

When the gripper grasped spheres of different diameters, the results are similar to those that we observed for the cylinders [see Fig. 6(b1)]. The peak forces stop increasing when the pressure reaches a threshold value because of the wall buckling effect [see Fig. 6(b2)]. For the 48 mm sphere, this value is -20 kPa, while for the 40 and 32 mm spheres, the value is -30 kPa. Comparing the results shown in Fig. 6(a) and (b), the forces produced when gripping the spheres are smaller than those for similarly sized cylinders at the same pressure. Thus, apart from the size, the lifting force produced by the gripper also depends on the shape of the grasped objects, as expected. This is also confirmed in the results shown in Fig. 6(c). At the same driving pressure (-30 kPa), the peak forces are different for each of the rectangular pyramid, the cone and the cube. When the gripper graspes the rectangular pyramid and cone, the peak forces also change significantly when the objects are grasped upside down. For the rectangular pyramid with the larger area facing down [the second object from the left in Fig. 6(c)], the peak force is nearly four times of that when the object is upside down [see leftmost object in Fig. 6(c)].

We also performed experiments to evaluate the extent of shear force enhancement produced by the gecko-like skin on different surface roughnesses. The results are shown in Fig. 6(d). When grasping the ABS cylinder, the peak forces of the gripper with gecko-like skin were nearly twice those of the gripper that lacked the skin. Thus, the gecko-like skin indeed augmented the shear force capacity. When the steel cylinder was grasped, the peak forces of the gripper with gecko-like skin were larger than those produced when grasping the ABS cylinder. However, the differences were small, suggesting that such a gecko-like

This article has been accepted for inclusion in a future issue of this journal. Content is final as presented, with the exception of pagination.

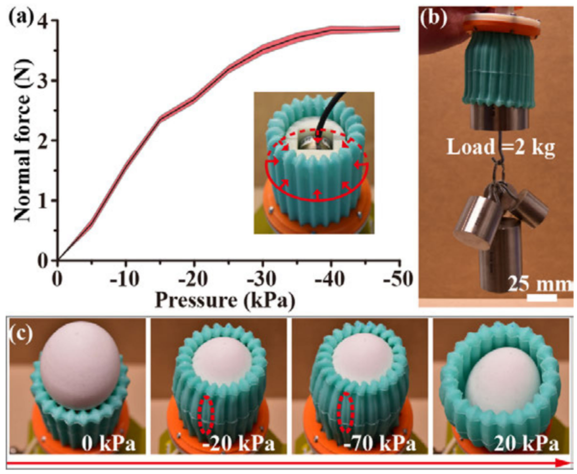

Fig. 5. Gripper can not only produce substantial lifting forces, but can also safely handle fragile objects by virtue of a wall buckling process. (a) Squeezing forces are produced through the application of vacuum pressure. During object grasping, the forces increase little beyond a vacuum pressure level of −30 kPa, at which point the interior chambers buckle and collapse, ensuring safe grasping. The diameter of the object is 32 mm. (b) Gripper can lift a weight of 2 kg owning to the gecko-like adhesion. (c) Gripper does not crush the egg even under the application of high vacuum pressures due to the buckling effect. The red dashed line illustrates the collapse of a chamber.

skin is effective in most dry surface conditions. It is worth noting that when the pressure was 0 kPa, large peak forces are produced provided that the diameters of the objects are larger than the uninflated interior diameter of the gripper [see Fig. 6(a2), (b2), and (d)]. For example, in Fig. 6(d), the peak forces of the gripper with gecko-like skin are nearly 20 N. This occurs because when grasping an object with a diameter larger than the nominal uninflated diameter of the gripper, the gripper is stretched through contact with the target. This compresses the gecko-like skin and yields friction forces sufficient to lift the object.

D. Lifting Forces During Expansion-Based Grasping

We evaluated the lifting forces of the gripper produced via the expansion-based grasping when grasping a hollow cylinder and a cube at different inflation pressures. The maximum forces increase linearly with pressure for both object shapes [see Fig. 6(e)]. This occurs because larger air pressures produce larger normal forces with the object, thus increasing the maximum shear force produced via friction. At identical fluid pressures, the lifting forces for the cylinder are larger than those for the cube. This suggests that the maximum lifting force depends on the shape and surface area of contact with the object, as would be expected from mechanical and tribological considerations. While there is no gecko-like skin on the exterior surface of the tested prototype grippers, such a skin could be applied to the exterior surface to augment lifting forces.

E. Gripping Flat Objects via Expansion-Driven Suction

We augment the gripper with a lip at the opening that enables the gripper to produce suction sufficient for lifting flat objects. Suction is generated through volume changes in the region enclosed by the inner surface of the gripper [see Fig. 7(a1) and (a2)]. As the pressure of the chambers P_C is increased, a moment is generated that produces a downward tilt in the outer rim of the lip. The lip bends to contact the flat surface, forming a seal with the interior space. As P_C continues to increase, the gripper inflates, yielding an increase in the enclosed volume, thereby decreasing the pressure P_I in the enclosed cavity, generating suction. The wedged shape of the lip ensures that the exterior part contacts the surface first, avoiding wrinkling, or other local deformations that would inhibit seal formation. Because the gripper is soft, the volume of the enclosed region increases further as the gripper is loaded during object lifting, enhancing the suction force [see Fig. 7(b)]. We measured the variation in suction force with the fluid pressure supplied to the gripper chambers. The suction force increases as the gripper is raised, before abruptly decreasing to zero when the maximum attainable force that it can exert on the surface is reached. If no seal is formed, the maximum lifting force that can be generated is small, 2 N. When a seal is formed, a greater lifting force of 15 N is attained even without the application of fluid pressure to the gripper [see Fig. 7(c1)], demonstrating that pulling the gripper upward after sealing generates suction through the expansion that is produced in the interior volume via lifting. When the gripper chambers are pressurized, greater suction is produced, yielding maximum lifting force of nearly 30 N at 20 kPa [see Fig. 7(c2)].

F. Multimodal Grasping

We conducted experiments on grasping a large variety of objects using the three different strategies. When grasping objects via contraction-based mode, the gripper was inflated to a maximum pressure of 40 kPa, and subsequently deflated to −40 kPa to enclose the objects. Results from Fig. 8(a) shows that the gripper can grasp a large camera clamp (1 kg), a bottle, scissors, a soldering clamp, a ruler, a bundle of pens, or a grape using the same simple behavior. Using the gecko-like skin, it can grasp a light bulb via the convex upper surface, without fully enclosing middle of the object. Grasping can be achieved provided the object, or a protuberant part of the object, is within the workspace of the gripper and the weight does not exceed the force capacity (which depends on the object geometry, see above). Via the expansion-based grasping mode, the gripper is inserted within an inner surface, handle, or aperture and inflated in order to produce grasp forces. Using this mode, the gripper can grasp a water dispenser barrel, a light bulb, a beaker, or a hollow cube via different openings in each [see Fig. 8(b)]. This only requires that a suitable cavity exists in which the gripper can be inserted. In Supplementary Video S3, we show how the gripper is able to perform these operations. We also show how, for some objects, multiple successful grasp strategies exist, through which the gripper conforms to different protuberances, achieving grasping via expansion or contraction. Fig. 8(c) shows that inflating the gripper enables it to use suction to attach to a variety of objects with flat surfaces: a box, a plate, a silicon wafer, or a mobile phone. The process through which each of

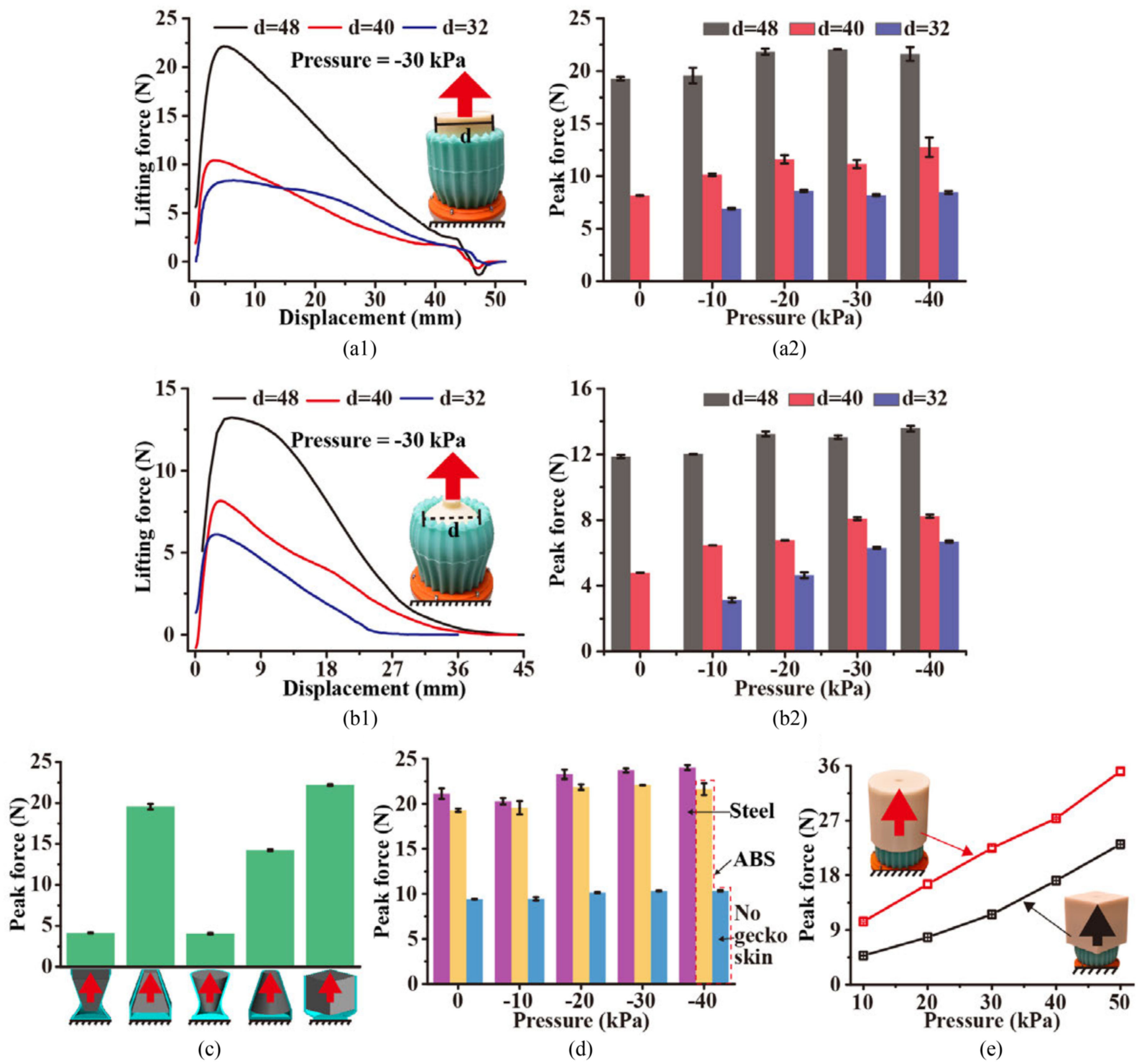

Fig. 6. Force results for the gripper. (a1) Measured force as the cylinders of different diameters are gradually pulled up out of the gripper. The air pressure is constant, −30 kPa, for all the objects. (a2) Peak forces for the three cylinders under different air pressures. (b1) Measured force as the spheres of different diameters are gradually pulled upward out of the gripper. The air pressure is −30 kPa for all the objects. (b2) Peak forces for the three spheres with varying fluid pressures. (c) Peak forces for objects of different shapes and poses at fixed pressure −30 kPa. All the objects have the same inscribed circle. (d) Comparison of the peak forces when the gripper grasps the 48 mm cylinders with different surface roughness (steel and 3D printed ABS), and when the grippers with gecko-like skin and without it grasp the same ABS cylinder. The diameters of the cylinders are 48 mm. (e) Peak forces of the cylinder and the square in the expansion-based grasping mode. The inner diameter of the cylinder and the inner width of the cube are both 48 mm.

these objects was grasped is shown in Supplementary Video S4. In summary, our gripper is able to grasp a wide range of objects with no requirement for calculations to find the feasible grasping points, greatly simplifying the process.

V. Discussion

A. Design Analysis

The analytical model was intended to predict the expansion of the aperture of the gripper. This determines the maximum size of the object that can be grasped. The results show good qualitative agreement with both the simulation and experiments across a wide range of fluidic pressures [see Fig. 3(b1) and (b2)]. The analytical model is also applicable for modeling grippers with different numbers of chambers, or alternative configurations [see Fig. 3(b3)]. It can help to determine the number of chambers required based on the maximum object size to be grasped. It nonetheless possesses some limitations. Because this model involves nonlinear equations, we determined approximate solutions via boundary conditions we imposed based on the symmetries of the physical motion. If the size of the chamber was changed, these assumptions may need revision. Moreover, the analytical model is based on the hypothesis that the specified top and bottom perimeter locations are fixed [see Fig. 3(a2)]. However, as our results suggest, these locations can be expected to displace when the air pressure is sufficiently large. Here, the model performed well for pressures up to 40 kPa. In alternative gripper designs, it is recommended to increase the height of the chambers, to reduce the constraints produced by the fasteners on

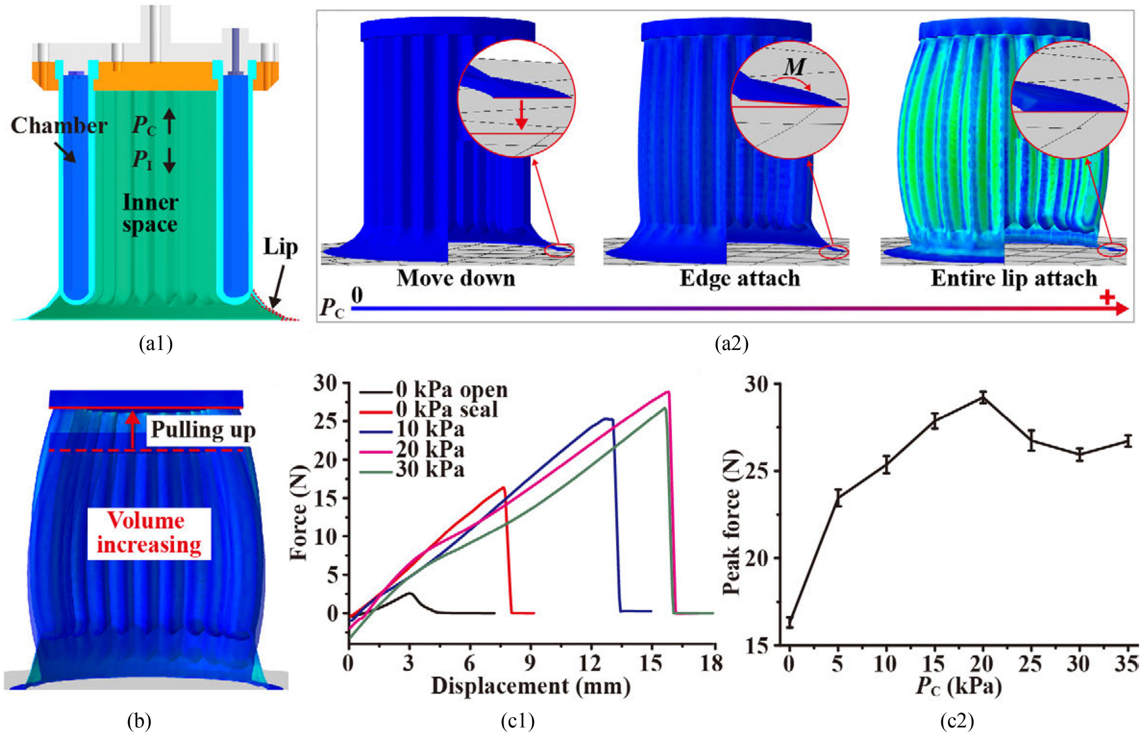

Fig. 7. Expansion-driven suction mode of grasping. (a1) Operating principle. When the gripper is inflated, the pressure P_C of the chambers increases, causing the lip to form a seal with the inner space. As the volume of the inner space increases, the pressure P_I inside that space decreases. (a2) FEA simulation shows how the seal is generated via inflation. (b) Because the gripper is soft, the volume of the inner space increases further when the gripper is raised, enhancing the suction force. (c1) Force versus pressure P_C as the gripper is raised. (c2) Peak forces observed at different pressures P_C.

the motion of the chambers. This may be important when more chambers are required.

B. Shape Conformation, Wall Buckling, and Gecko-inspired Adhesion

Three main factors affect the grasping ability of grippers: achieving sufficient effective area of contact, ensuring sufficiently soft contact to prevent damaging handled objects, and providing sufficient strength to achieve the required load capacity. The bending behavior of fingered grippers typically impedes their fingers from touching a surface between support points. In addition, the number and orientations of the fingers constrains the feasible grasp locations. Both of these aspects complicate grasp planning and grasping [see Fig. 4(a1) and (a2)]. In contrast, our device is able to conform to objects of different sizes and shapes by means of a inflation or deflation supplied via a single fluidic port [see Fig. 4(a3) to (g)]. This increases the stability of grasping and simplifies grasp planning.

Grippers often require sufficient softness to enable them to handle fragile items, and sufficient stiffness for lifting heavy objects. One solution to this challenge is to dynamically control gripper stiffness [22], [28], [29]. However, increasing stiffness can negatively impact safety, causing a gripper to damage fragile objects, can complicate their control, and may also degrade the ability of such a gripper to conform to objects. In our design, a wall buckling mechanism ensures that the gripper does not produce excessive squeeze forces when negative pressures are applied [see Fig. 5(a) and Fig. 6(a2), (b2), and (d)]. This ensures that the gripper can safely grasp fragile objects [see Fig. 5(c)]. The gecko-like skin patterned on the interior surface enables the gripper to lift weights up to 20 N [see Fig. 5(b)]. Such loads are often prohibitively large for silicone rubber grippers to lift [19]. The gecko-like skin not only increases the shear force capacity, but also enables the gripper to manipulate some large objects without the application of fluid energy [see Fig. 6(a2), (b2), and (d)]. The combination of wall bucking and gecko-inspired adhesion combine to ensure both safety and sufficient load capacity.

C. Multimodal Grasping

Our gripper possesses key properties, compliant shape-adaptation, wall buckling, and gecko-like adhesion, that enable it to grasp multiple objects when driven via a simple inflating-deflating control from a single fluidic port (see Fig. 8). The gripper can adapt to the geometry of many objects by passively conforming to them, without accounting for the detailed object geometry or pose. Wall buckling ensures that the air pressure need not be continuously adjusted to regulate the grasping force. The gecko-like surface improves load capacity, and aids the gripper in producing lifting forces without the addition of fluidic energy. Compared to other nonanthropomorphic, vacuum-driven grippers, which typically can only grasp objects under negative pressure [34]–[36], our gripper can adopt multiple grasping strategies, using its inner or outer surfaces. The main

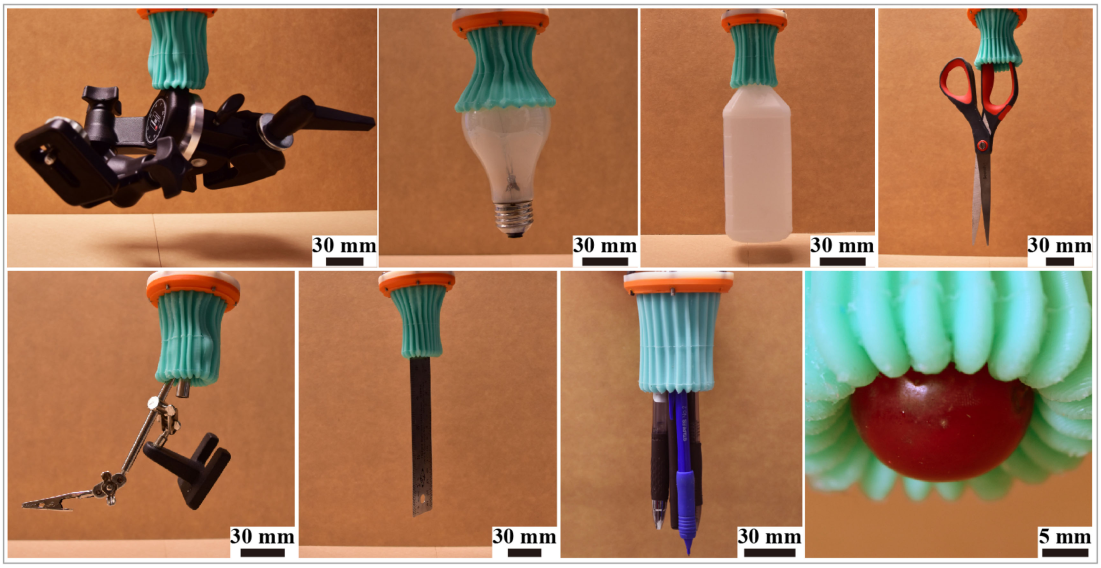

(a)

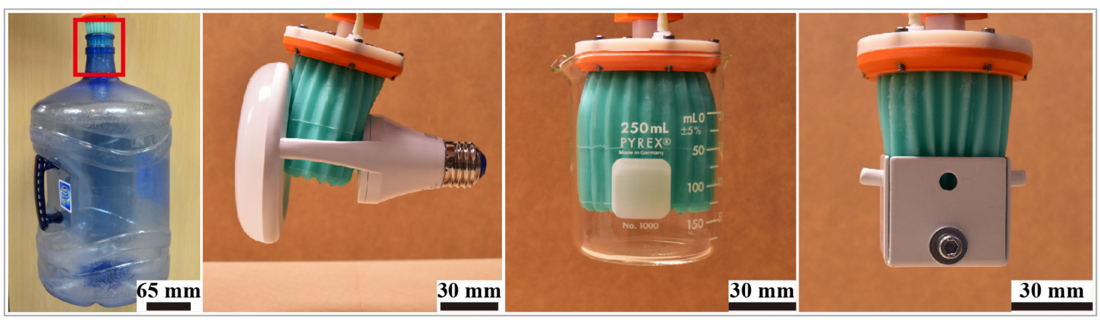

(b)

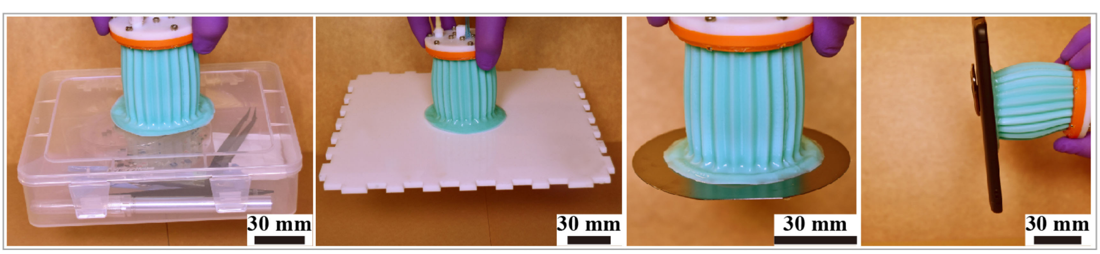

(c)

Fig. 8. Examples of the performance of the gripper in different grasping modes. (a) Contraction-based grasping of a large camera clamp (1 kg), a light bulb, a bottle of isopropyl alcohol (400 g), scissors, a soldering clamp, a ruler, a bundle of pens, or a grape. (b) Expansion-based grasping of a water dispenser barrel, a light bulb, a beaker, or a hollow cube. (c) Expansion-driven suction based grasping of a box containing several objects, an acrylic plate, a silicon wafer, and a mobile phone.

considerations affecting the operation of such a gripper is that the object dimensions and weight lie within the feasible range for the respective gripper. In contrast, in order for a fingered gripper (whether soft or rigid) to grasp complex objects (e.g., scissors, soldering clamps, or rulers in our object set), complicated computations would be required in order to achieve force/form closure, and thus stable grasping. Such grippers must also typically be continuously controlled so that appropriate grasp forces are maintained. Furthermore, it is difficult for a fingered gripper to grasp an object via the interior of an orifice if the orifice is smaller than the gripper. In contrast, our gripper can be deflated to a smaller size and be inserted into the orifice and subsequently inflated to a larger size. This enables it to exert forces against the inner surface of the orifice that are sufficient for lifting. Another advantage of our expansion-driven suction method of grasping is that the gripper can attach to and lift flat objects without continuous vacuuming. Suction can be generated via the low-volume inflation of the gripper. As we demonstrate, this is achieved using the same fluidic port that is used for the contraction and expansion operating, without added complexity. The parsimonious design enables our gripper to perform multiple grasping behaviors that can be driven via its single fluidic input. It is, thus, amenable to many practical applications.

D. Failure Modes

Although this gripper design can grasp a variety of objects using multiple grasping strategies, there are several limitations that can lead to grasp failure. First, the gripper is designed to envelop and lift objects in an upward manner in which the gripper symmetry axis is approximately aligned with vertical. Lifting large loads in poses inclined with the vertical can fail due to the low lateral stiffness. Second, similar to other soft grippers, the size and weight of grasped objects must be within a feasible range to achieve a successful grasping. We believe that the range can be improved by changing the number of chambers (as supported by our analyses) or via scaling gripper dimensions (as we intend to analyze in future work). Thus, for example, the gripper cannot easily grasp a small elongated object, such as a pen. Gripping such an object in poses when it cannot be enveloped, such as when it is lying on a table, is likewise challenging. Third, in suction mode, an adequate seal between the gripper lip and surface must be achieved. Thus, the gripper cannot readily lift an object by applying suction to a flat but highly corrugated surface. In our current prototype, the presence of a lip may also introduce adverse effects for the other two modes due to collisions with object features (depending on detailed object shape). We believe this can be improved, if application requirements demand, by optimizing the lip geometry (for example, using a thinner lip), or through the use of a modular lip attachment.

VI. Conclusion

In summary, this article presented a new fingerless soft gripper capable of efficiently generating multiple grasping modes. It is based on a soft accordion structure containing coupled, parallel fluidic chambers. This structure allowed us the gripper to passively adapt its shape to conform to grasped objects. It was controlled via pressure supplied from a single fluidic port. Inflation opens the gripper orifice for enveloping an object, while deflation produces grasping forces. The interior was patterned with a gecko-like skin that increases friction, enabling the gripper to lift objects weighing up to 20 N without continuously applied power. Our design ensures that fragile objects, such as eggs, can be safely handled by virtue of a wall buckling mechanism. The gripper also admits a mode of grasping in which it may be inflated within an opening or orifice. This enables it to grasp objects with handles or openings. We also showed how the design of an integrated lip allows the gripper to form a seal, and, upon inflating, to generate suction sufficient to lift many flat objects. This simple design, thus, integrates features that ensure it can conform to many objects via different features or flat surfaces.

The parsimonious combination of the features, and the grasping modes they enable, allows this gripper design to solve many grasping tasks via a single fluidic input. This design is amenable for use in a wide range of tasks. Such devices could improve the ability of robotic systems to meet application needs in areas of great economic and societal importance. Some potential application domains include food processing, logistical sorting, including pick-and-place sorting of heterogeneous objects on an assembly line. There are many opportunities for further extending the ideas presented here, in order to expand the workspace and capacity of the gripper. Such improvements could further expand the range of applications of such devices.

References

[1] C. Melchiorri and M. Kaneko, "Robot hands," in *Springer Handbook of Robotics*. New York, NY, USA: Springer, 2008, pp. 345–360.
[2] R. Paolini, A. Rodriguez, S. S. Srinivasa, and M. T. Mason, "A data-driven statistical framework for post-grasp manipulation," *Int. J. Robot. Res.*, vol. 33, no. 4, pp. 600–615, 2014.
[3] N. S. Pollard, "Closure and quality equivalence for efficient synthesis of grasps from examples," *Int. J. Robot. Res.*, vol. 23, no. 6, pp. 595–613, 2004.
[4] F. Ficuciello, A. Migliozzi, G. Laudante, P. Falco, and B. Siciliano, "Vision-based grasp learning of an anthropomorphic hand-arm system in a synergy-based control framework," *Sci. Robot.*, vol. 4, 2019, Art. no. eaao4900.
[5] J. Shintake, V. Cacucciolo, D. Floreano, and H. Shea, "Soft robotic grippers," *Adv. Mater.*, vol. 30, no. 29, 2018, Art. no. 1707035.
[6] J. Shintake, S. Rosset, B. Schubert, D. Floreano, and H. Shea, "Versatile soft grippers with intrinsic electroadhesion based on multifunctional polymer actuators," *Adv. Mater.*, vol. 28, no. 2, pp. 231–238, 2016.
[7] G.-K. Lau, K.-R. Heng, A. S. Ahmed, and M. Shrestha, "Dielectric elastomer fingers for versatile grasping and nimble pinching," *Appl. Phys. Lett.*, vol. 110, no. 18, 2017, Art. no. 182906.
[8] S. Shian, K. Bertoldi, and D. R. Clarke, "Dielectric elastomer based "grippers" for soft robotics," *Adv. Mater.*, vol. 27, no. 43, pp. 6814–6819, 2015.
[9] T. N. Do, H. Phan, T.-Q. Nguyen, and Y. Visell, "Miniature soft electromagnetic actuators for robotic applications," *Adv. Functional Mater.*, vol. 28, no. 18, 2018, Art. no. 1800244.
[10] E. Diller and M. Sitti, "Three-dimensional programmable assembly by untethered magnetic robotic micro-grippers," *Adv. Functional Mater.*, vol. 24, no. 28, pp. 4397–4404, 2014.
[11] A. M. Hubbard, E. Luong, A. Ratanaphruks, R. W. Mailen, J. Genzer, and M. D. Dickey, "Shrink films get a grip," *ACS Appl. Polym. Mater.*, vol. 1, no. 5, pp. 1088–1095, 2019.
[12] J. C. Breger *et al.*, "Self-folding thermo-magnetically responsive soft microgrippers," *ACS Appl. Mater. Interfaces*, vol. 7, no. 5, pp. 3398–3405, 2015.
[13] M. Pilz da Cunha *et al.*, "An untethered magnetic-and light-responsive rotary gripper: Shedding light on photoresponsive liquid crystal actuators," *Adv. Opt. Mater.*, vol. 7, no. 7, 2019, Art. no. 1801643.
[14] A. M. Abdullah, X. Li, P. V. Braun, J. A. Rogers, and K. J. Hsia, "Self-folded gripper-like architectures from stimuli-responsive bilayers," *Adv. Mater.*, vol. 30, no. 31, 2018, Art. no. 1801669.
[15] S. Y. Zheng *et al.*, "Programmed deformations of 3d-printed tough physical hydrogels with high response speed and large output force," *Adv. Functional Mater.*, vol. 28, no. 37, 2018, Art. no. 1803366.
[16] B. Mosadegh *et al.*, "Pneumatic networks for soft robotics that actuate rapidly," *Adv. Functional Mater.*, vol. 24, no. 15, pp. 2163–2170, 2014.
[17] N. K. Uppalapati and G. Krishnan, "Towards pneumatic spiral grippers: Modeling and design considerations," *Soft Robot.*, vol. 5, no. 6, pp. 695–709, 2018.
[18] C. Tawk, M. in het Panhuis, G. M. Spinks, and G. Alici, "Bioinspired 3d printable soft vacuum actuators for locomotion robots, grippers and artificial muscles," *Soft Robot.*, vol. 5, no. 6, pp. 685–694, 2018.
[19] Y. Hao *et al.*, "A soft bionic gripper with variable effective length," *J. Bionic Eng.*, vol. 15, no. 2, pp. 220–235, 2018.
[20] K. C. Galloway *et al.*, "Soft robotic grippers for biological sampling on deep reefs," *Soft Robot.*, vol. 3, no. 1, pp. 23–33, 2016.
[21] H. Yuk, S. Lin, C. Ma, M. Takaffoli, N. X. Fang, and X. Zhao, "Hydraulic hydrogel actuators and robots optically and sonically camouflaged in water," *Nat. Commun.*, vol. 8, 2017, Art. no. 14230.
[22] Y. Hao *et al.*, "A eutectic-alloy-infused soft actuator with sensing, tunable degrees of freedom, and stiffness properties," *J. Micromech. Microeng*, vol. 28, no. 2, 2018, Art. no. 024004.
[23] J. Zhou, J. Yi, X. Chen, Z. Liu, and Z. Wang, "BCL-13: A 13-DOF soft robotic hand for dexterous grasping and in-hand manipulation," *IEEE Robot. Autom. Lett.*, vol. 3, no. 4, pp. 3379–3386, Oct. 2018.

[24] Y. Yang, Y. Chen, Y. Li, M. Z. Chen, and Y. Wei, "Bioinspired robotic fingers based on pneumatic actuator and 3d printing of smart material," *Soft Robot.*, vol. 4, no. 2, pp. 147–162, 2017.
[25] Y. Wei *et al.*, "A novel, variable stiffness robotic gripper based on integrated soft actuating and particle jamming," *Soft Robot.*, vol. 3, no. 3, pp. 134–143, 2016.
[26] Y. Jiang, D. Chen, C. Liu, and J. Li, "Chain-like granular jamming: A novel stiffness-programmable mechanism for soft robotics," *Soft Robot.*, vol. 6, no. 1, pp. 118–132, 2019.
[27] H. K. Yap, H. Y. Ng, and C.-H. Yeow, "High-force soft printable pneumatics for soft robotic applications," *Soft Robot.*, vol. 3, no. 3, pp. 144–158, 2016.
[28] M. Zhu, Y. Mori, T. Wakayama, A. Wada, and S. Kawamura, "A fully multi-material three-dimensional printed soft gripper with variable stiffness for robust grasping," *Soft Robot.*, vol. 6, pp. 507–519, 2019.
[29] Y.-F. Zhang *et al.*, "Fast-response, stiffness-tunable soft actuator by hybrid multimaterial 3d printing," *Adv. Functional Mater.*, vol. 29, no. 15, 2019, Art. no. 1806698.
[30] K. Yamaguchi, Y. Hirata, and K. Kosuge, "Development of robot hand with suction mechanism for robust and dexterous grasping," in *Proc. IEEE/RSJ Int. Conf. Intell. Robots and Syst.*, 2013, pp. 5500–5505.
[31] H. S. Stuart, S. Wang, B. Gardineer, D. L. Christensen, D. M. Aukes, and M. Cutkosky, "A compliant underactuated hand with suction flow for underwater mobile manipulation," in *Proc. IEEE Int. Conf. Robot. Autom.*, 2014, pp. 6691–6697.
[32] S. Hasegawa, K. Wada, Y. Niitani, K. Okada, and M. Inaba, "A three-fingered hand with a suction gripping system for picking various objects in cluttered narrow space," in *Proc. IEEE/RSJ Int. Conf. Intell. Robots Syst.*, 2017, pp. 1164–1171.
[33] 2020. [Online]. Available: https://www.righthandrobotics.com/
[34] E. Brown *et al.*, "Universal robotic gripper based on the jamming of granular material," *Proc. Nat. Acad. Sci.*, vol. 107, no. 44, pp. 18809–18814, 2010.
[35] J. R. Amend, E. Brown, N. Rodenberg, H. M. Jaeger, and H. Lipson, "A positive pressure universal gripper based on the jamming of granular material," *IEEE Trans. Robot.*, vol. 28, no. 2, pp. 341–350, Apr. 2012.
[36] S. Li *et al.*, "A vacuum-driven origami 'magic-ball' soft gripper," in *Proc. IEEE Int Conf Robot. Autom.*, May 2019, pp. 7401–7408.
[37] F. Tramacere, L. Beccai, F. Mattioli, E. Sinibaldi, and B. Mazzolai, "Artificial adhesion mechanisms inspired by octopus suckers," in *Proc. IEEE Int. Conf. Robot. Autom.*, 2012, pp. 3846–3851.
[38] J. A. Sandoval, S. Jadhav, H. Quan, D. D. Deheyn, and M. T. Tolley, "Reversible adhesion to rough surfaces both in and out of water, inspired by the clingfish suction disc," *Bioinspiration Biomimetics*, vol. 14, no. 6, 2019, Art. no. 066016.
[39] Y. Wang *et al.*, "A biorobotic adhesive disc for underwater hitchhiking inspired by the remora suckerfish," *Sci. Robot.*, vol. 2, no. 10, 2017, Art. no. eaan8072.
[40] Y. Okuno, H. Shigemune, Y. Kuwajima, and S. Maeda, "Stretchable suction cup with electroadhesion," *Adv. Mater. Technol.*, vol. 4, no. 1, 2019, Art. no. 1800304.
[41] Z. Zhakypov, F. Heremans, A. Billard, and J. Paik, "An origami-inspired reconfigurable suction gripper for picking objects with variable shape and size," *IEEE Robot. Autom. Lett.*, vol. 3, no. 4, pp. 2894–2901, Oct. 2018.
[42] E. W. Hawkes, H. Jiang, D. L. Christensen, A. K. Han, and M. R. Cutkosky, "Grasping without squeezing: Design and modeling of shear-activated grippers," *IEEE Trans. Robot.*, vol. 34, no. 2, pp. 303–316, Apr. 2018.
[43] P. Day, E. V. Eason, N. Esparza, D. Christensen, and M. Cutkosky, "Microwedge machining for the manufacture of directional dry adhesives," *J. Micro Nano-Manuf.*, vol. 1, no. 1, 2013, Art. no. 011001.
[44] N. Kidambi, R. L. Harne, and K.-W. Wang, "Modular and programmable material systems drawing from the architecture of skeletal muscle," *Phys. Rev. E*, vol. 98, no. 4, 2018, Art. no. 043001.

Yufei Hao received the B.S. degree in mechanical engineering from the Hebei University of Technology, Tianjin, China, in 2013, and the Ph.D. degree in mechatronic engineering from Beihang University, Beijing, China, in 2020.

He is currently a Postdoctoral Fellow with Soft Transducers Laboratory, École Polytechnique Fédérale de Lausanne. His research interests include smart materials, robotic design, soft robotic grasping, and soft sensors.

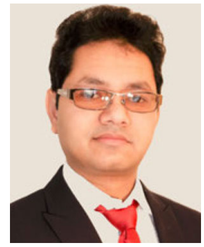

Shantonu Biswas received the B.Sc. degree in physics from the Shahjalal University of Science and Technology, Sylhet, Bangladesh, the M.Sc. degree in physics from the Lund University, Lund, Sweden, in 2013, and the Ph.D. (Hons.) degree in nanotechnology from the Department of Nanotechnology, Ilmenau University of Technology, Ilmenau, Germany, in 2018.

He is a Postdoctoral Fellow with the RE Touch Lab, California NanoSystems Institute, University of California, Santa Barbara, CA, USA. He invented a novel stretchable printed circuit board method with the Department of Nanotechnology, Ilmenau University of Technology. His research interests include flexible, wearable and stretchable electronics, nanotechnology, materials engineering, bioengineering, and digital manufacturing.

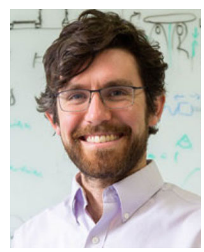

Elliot Wright Hawkes (Member, IEEE) received the A.B. (Hons.) degree in mechanical engineering from Harvard University, Cambridge, MA, USA, in 2009, and the M.S. and Ph.D. degrees in mechanical engineering from Stanford University, Stanford, CA, USA, in 2012 and 2015, respectively.

He is an Assistant Professor with the Department of Mechanical Engineering, University of California, Santa Barbara, USA. His research interests include compliant robot design, mechanism design, nontraditional materials, artificial muscles, directional adhesion, and growing robots.

Dr. Hawkes was the recipient of the National Science Foundation CAREER Award and the NASA Early Faculty Career Award.

Tianmiao Wang received the B.E. degree from Xi'an Jiaotong University, Xi'an, China, in 1982, and the M.E. and Ph.D. degrees from Northwestern Polytechnic University, Xi'an, in 1984 and 1990, respectively, all in computer science.

He is currently the Dean and a Professor with the School of Mechanical Engineering and Automation, Beihang University, Beijing. He is also the Head of the Expertized Group in the field of advanced manufacturing the technology of the National High Technology Research and Development Program (863 Hi-Tech Program). He has undertaken and finished many national research projects in recent years. He has authored and coauthored more than 150 articles in local and international journals and four professional books. His research interests include biomimetic robotics, medical robotics technology, and embedded intelligent control technology.

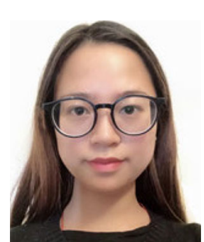

Mengjia Zhu received the B.Eng. (Hons.) degree in apparel design and engineering from Soochow University, Suzhou, China, in 2015, and the M.S. degree in materials science and engineering from Arizona State University, Tempe, AZ, USA, in 2017. She is currently working toward the Ph.D. degree in media arts and technology with the University of California, Santa Barbara, Santa Barbara, CA, USA, under the supervision of Prof. Y. Visell.

Her research interests include the design and fabrication of soft robots, functional wearables, and haptics.

Li Wen received the B.E. degree in mechatronics engineering from the Beijing Institute of Technology, Beijing, China, in 2005, and the Ph.D. degree in mechanical engineering from Beihang University, Beijing, in 2011.

He was a Postdoctoral Fellow with Harvard University, Cambridge, MA, USA, from 2011 to 2013. He is currently a Full Professor with Beihang University. His research interests mainly include bioinspired robotics, soft robotics, and comparative biomechanics.

Prof. Wen is the Associate Editor for Soft Robotics and the IEEE ROBOTICS AND AUTOMATION LETTERS. He is an Editorial Board Member of Bioinspiration Biomimetics, and the Academic Editor of PLOS ONE.

Yon Visell received the B.A. degree in physics from the Wesleyan University, Middletown, CT, USA, in 1995, and the M.A. degree in physics from The University of Texas, Austin, Austin, TX, USA, in 1999, and the Ph.D. degree in electrical and computer engineering from McGill University, Montreal, QC, Canada, in 2011.

He is currently an Associate Professor with the University of California, Santa Barbara, Santa Barbara, CA, USA, in the Media Arts and Technology Program, Department of Electrical and Computer Engineering, and Department of Mechanical Engineering (by courtesy). His academic interests include haptics, soft robotics, and soft electronics. He was a Postdoctoral Scholar with Sorbonne University, Paris. Prior to his Ph.D. studies, Visell spent several years in industry positions, including that of DSP developer for Ableton Live. He has authored and coauthored more than 75 scientific works.

Dr. Visell was the recipient of several awards for work presented at prominent academic conferences. He received a Google Faculty Research Award in 2016, a Hellman Family Foundation Faculty Fellowship in 2017, and a U.S. National Science Foundation CAREER award in 2018. He is an Associate Editor for the IEEE ROBOTICS AND AUTOMATION LETTERS and serves as General Co-Chair of the 2022 IEEE Haptics Symposium.